Available online at www.sciencedirect.com
ScienceDirect
Microelectronics Reliability 48 (2008) 245–260
MICROELECTRONICS RELIABILITY
www.elsevier.com/locate/microrel

Organic substrates for flip-chip design: A thermo-mechanical model that accounts for heterogeneity and anisotropy

L. Valdevit [a,*], V. Khanna [a], A. Sharma [a], S. Sri-Jayantha [a], D. Questad [b], K. Sikka [b]

[a] IBM Corporation, T. J. Watson Research Center, Yorktown Heights, NY 10598, United States
[b] IBM Corporation, Systems and Technology Group, Hopewell Junction, NY 12533, United States

Received 11 December 2006; received in revised form 15 February 2007
Available online 17 May 2007

Abstract

We present a thermo-mechanical characterization of organic substrates that accounts for heterogeneity both in the in-plane and out-of-plane directions. Systematic observation of the board files of a number of substrates of commercial interest reveals primarily three recurrent topological arrangements of copper and polymer; for each arrangement, the in-plane effective thermo-elastic properties are calculated via appropriate composite materials models. The averaging process in the out-of-plane direction (i.e. the stacking effect) is performed using standard laminated plate theory. The model is successfully applied to various regions of three organic substrates of interest (mainly differing in core thickness): the analytically calculated effective Young's moduli (E) and coefficients of thermal expansion (CTE) are shown to be typically within 10% of the experimental measurements. An important attribute of this model is its ability to provide substrate description at various levels of complexity: a few effective properties are outputted that can be useful for further purely analytical investigations; at the same time, the model provides the full stiffness matrix for each region of the substrate, to be used for more detailed finite elements simulations of higher-level structures (e.g. silicon die/underfill/substrate/cooling solution assemblies). Preliminary application of this model to the warp analysis of a flip-chip is presented in the end.

1. Introduction

In the early days of the personal computer industry, wire bonding has been the primary technology employed to establish electrical connections of a chip with its substrate. Although appealing for its simplicity and low cost, this procedure has recently become inadequate for high-density interconnects. The flip-chip approach has become the technology of choice today: in this design, an array of solder joints, called C4 (controlled collapse chip connection), spans the whole area of the silicon die and provides high-density electrical connection to the substrate [1]. Ceramic substrates were initially used, but in 1997 Intel proved that the same connection density and superior dielectric properties could be achieved by sequential build-up (SBU) laminate organic substrates [2]. The notable cost reduction associated with organic substrates stimulated significant research efforts to address their main shortcoming: a severe thermal mismatch with the silicon die (a typical organic substrate has a coefficient of thermal expansion (CTE) 5–8 times larger than that of silicon). Upon temperature excursions of 100 °C or more, the thermal mismatch of die and substrate warps the assembly, imposing large stresses on the solder joints, and ultimately leading to fatigue failure after a number of cycles. The characterization of the solder joints fatigue life has occupied much of the technical literature in the packaging industry for the past few years [3–11]. Although experiments are important, analytical/computational models that can extrapolate experimental results to new die sizes and joints configurations are ultimately needed. All these models necessarily rely on accurate knowledge of the thermo-mechanical properties of the substrate.

An organic substrate is a highly heterogeneous structure, typically resulting from the stacking of a number of

* Corresponding author. Tel.: +1 805 893 4667; fax: +1 805 893 8486.
E-mail address: lorenzo@engineering.ucsb.edu (L. Valdevit).

0026-2714/$ - see front matter © 2007 Elsevier Ltd. All rights reserved.
doi:10.1016/j.microrel.2007.03.006

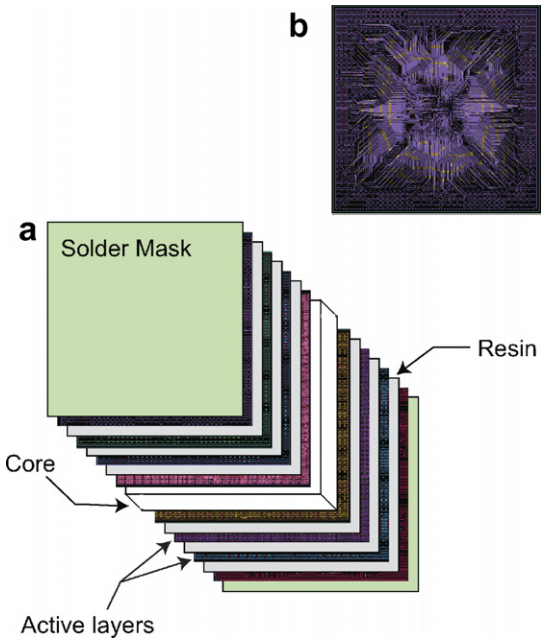

Fig. 1. (a) Schematic of the layer stack-up for a typical organic substrate (thicknesses not to scale). (b) Typical in-plane arrangement of a logical layer.

layers (15–21 layers, for the substrate analyzed in this work) at both sides of a structural core (Fig. 1a).

There are two categories of layers:

(i) 'active' layers (15–20 μm thick), with the function of transmitting the electrical signal (I/O) and/or providing access to a uniform voltage; from a mechanical perspective they are composite materials, with some regions mainly consisting of copper lines embedded in a polymeric matrix (resin), and others essentially made of pure copper with distributions of holes (vias);
(ii) passive resin layers (~30 μm thick), that electrically insulate the active layers from one another.

The core has the function of providing stiffness and strength to the substrate, while keeping the effective coefficient of thermal expansion low enough; the core thickness varies greatly from design to design, with a clear trend towards thinner cores: recent designs have core thicknesses of the order of 400 μm, while totally coreless substrates are being investigated. The electric advantage of coreless solutions is unfortunately coupled with a new series of thermo-mechanical challenges: the extremely low substrate stiffness translates in large strains, whereas the high coefficient of thermal expansion emphasizes the mismatch with the Silicon die. The successful manufacturing of these substrates heavily relies on modeling capabilities to guide the design.

A visual analysis of the board file of an organic substrate immediately reveals that even within a single layer there is significant heterogeneity and anisotropy (Fig. 1). The designer who wants to extract a set of effective properties is then faced with a dual challenge: in-plane and out-of-plane properties variation. This problem can be tackled at a variety of levels (Fig. 2); the main compromise, as usual, is between detail and complexity. For fully analytical studies of package warp and/or C4 fatigue failure, a minimal set of effective properties is needed [12–16]. Given the multi-layered nature of the organic substrates, a common approach adopts the theory of laminated plates, thus accounting for out-of-plane properties variations but neglecting any in-plane heterogeneity and/or anisotropy [17–19]. Although necessary to allow for analytical manipulations, this simplification is unnecessarily restrictive for finite elements (FE) studies of higher-level assemblies (e.g. complete flip-chip configurations, encompassing substrate, silicon die, underfill and thermal solutions). On the other hand, a full finite element representation of a 5 cm × 5 cm substrate, with the ability to resolve a single copper line or via (typical size of the order of a few microns), would require at least 10 billion elements, and is obviously impractical. Furthermore, the results could not be extrapolated to different substrate designs. These considerations clearly show the need for a thermo-mechanical characterization of the substrate that captures both its in-plane and out-of-plane heterogeneity and anisotropy, while retaining computational efficiency. Notable efforts in this direction have recently been taken [20–22]. In [20], Grenestedt and Hutapea investigated the in-plane anisotropy of a substrate where the logical layers present straight copper lines running alternatively along the 0° and 90° directions. They showed that simple composite materials models are sufficient to estimate the stiffness of each layer, irrespective of the layer build-up. In [21], Hutapea and Grenestedt improved their analysis, and calculated the effective properties of other morphological features typically present in logical layers (plated-though-holes, adhesion holes and micro-vias). This allowed the assembly of a homogenized finite element model of the whole substrate, capturing both in-plane and out-of-plane heterogeneity and anisotropy. In [22], Ubachs et al. introduced a fully automated approach that interprets the morphology of every region of each layer of the substrate by means of autocorrelation, calculating their copper content, degree of anisotropy and principal direction. Effective properties are then assigned to each region based on two very simple mechanical models. A global finite element model can be constructed using the effective properties calculated with this approach, and global/local schemes suitable for time-efficient but accurate stress estimates are demonstrated.

Here we present an analytical model that encompasses similar features; the proposed approach is *flexible* (both a minimal set of effective properties and a more extensive thermo-mechanical representation can be obtained), and *easy to use* (a new substrate can be analyzed with minimal user-input). The homogenization technique is similar to that presented in [21], although no single feature is resolved. Instead, each layer in the substrate is divided in tiles, and each tile is associated one of three possible

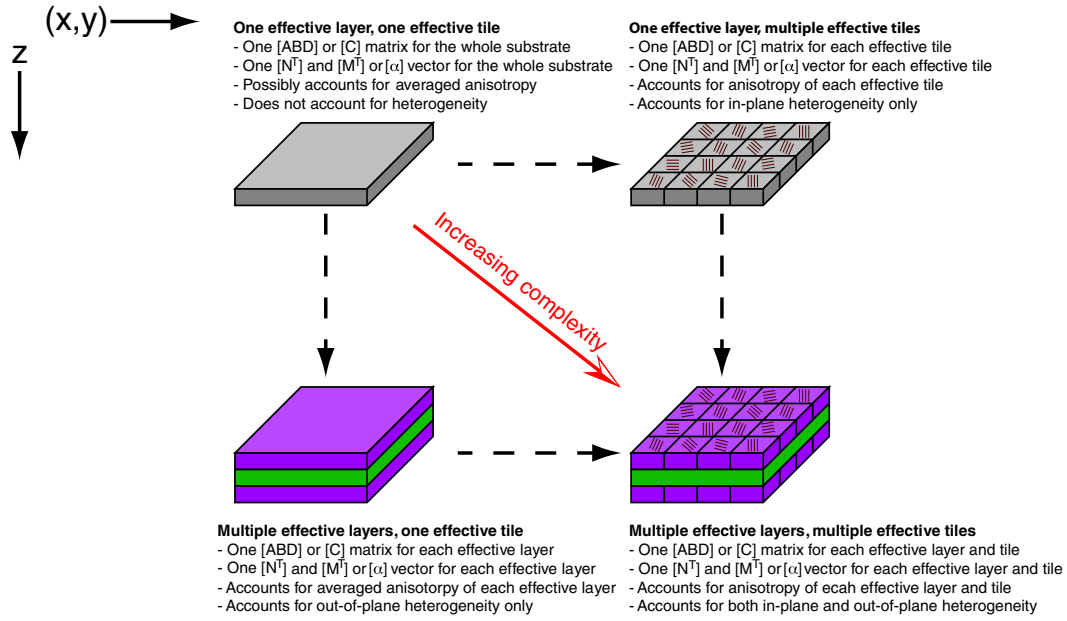

Fig. 2. Various modeling approaches for organic substrates. For every approach, the thermo-mechanical characterization can be provided either in terms of the $[ABD]$ matrix and the $[N^T]$ and $[M^T]$ vectors (Section 2, Eqs. (13)–(15)), or in terms of anisotropic thermo-mechanical properties via the $[C]$ matrix and $[\alpha]$ vector (Section 4, Eqs. (23)–(25)).

thermo-mechanical models: *lines*, *vias* or *web* (see Section 2 for details). Effective properties are calculated for each model, and standard laminated plate theory is used to assemble all the layers (upon rotation of each layer, as different tiles can have different feature orientations). The ability of this model to quantitatively capture heterogeneity and anisotropy is verified through a series of thermo-mechanical measurements on various test coupons extracted from three different substrates of commercial interest (mainly differing in core thickness). The spatial variation of the thermo-mechanical properties of such substrates is reported. We emphasize that this information can be used to guide the placement of various components (e.g. capacitors) in the chip. Finally, a global finite element model of the substrate based on the effective properties described above is assembled and used to predict warp of a flip-chip (encompassing Silicon die, underfill and substrate) upon a deep thermal cycle (DTC); this analysis clearly reveals the importance of substrate anisotropy and heterogeneity.

The outline of the paper is as follows. Section 2 presents the analytical model; Section 3 describes the experimental protocol and results. Useful information on the spatial variation of properties in these substrates (both in-plane and out-of-plane) is provided in Section 4. Section 5 applies the model to a finite elements (FE) warp analysis of a flip-chip. Conclusions follow.

2. Model description

The analytical model relies upon the theory of laminated plates, initially developed for the study of polymer-matrix fiber-reinforced composite materials [23]. Visual inspection of the logical layers of a typical organic substrate reveals a very fine-scale heterogeneity (Fig. 3): the topological arrangement and relative amounts of the two constituents (copper and resin) vary significantly in the plane of the layers, thus defying the application of a standard composite materials model to the whole layer. We address this problem by dividing each layer in a number of regions (tiles): as long as the tiles are sufficiently small, each of them has a fairly uniform copper content and its microstructure can be adequately represented by one of the following three models: (a) "lines", (b) "vias" or (c) "web" (Fig. 4). The copper content can be extracted for each tile by applying a custom-built image analysis software to the board file. Fig. 3 presents the outcome of this procedure for a medium-thickness core of practical interest: nine tiles were used, and copper content and topological features are presented for each tile in each active layer. Obviously, the accuracy of the method increases with the number of tiles, at the expense of user-time.

The effective thermo-elastic properties of each tile can then be calculated in a two-step process: (a) the effective properties of each layer within each tile are derived from the properties of the constituents, the layer topology and the copper content (see Section 2.1); (b) the theory of laminated plates is used to extract the effective properties of the laminate for each tile (see Section 2.2). Once the thermo-mechanical behavior of each tile has been characterized, the necessary set of properties needed for a heterogeneous and anisotropic finite elements representation of the substrate is readily extracted (see Section 5); at the same time, a simple averaging process will provide a minimal set of properties needed to characterize the substrate in further analytical calculations (see Section 2.3).

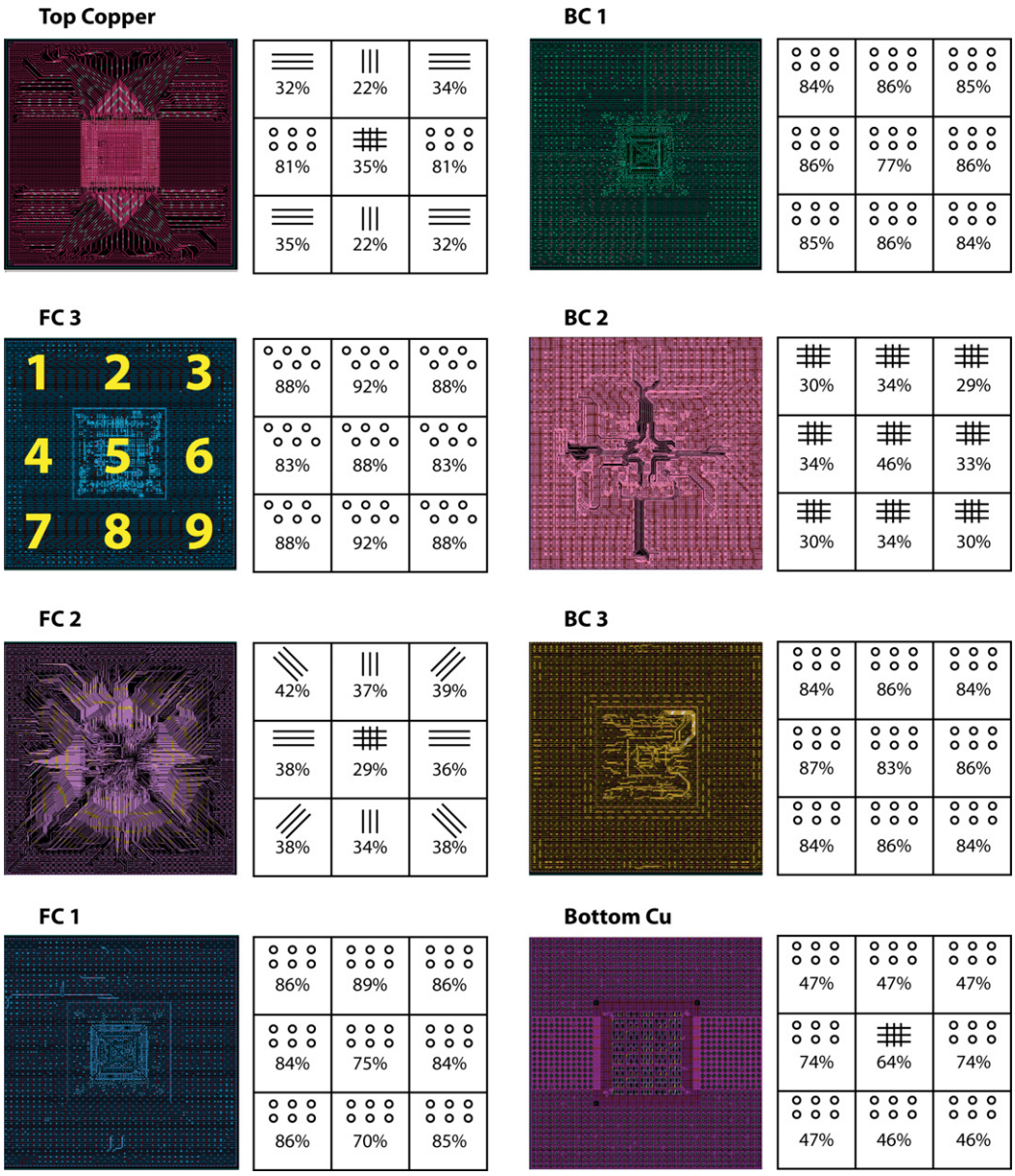

Fig. 3. Complete model of an organic substrate. Each layer was divided in nine tiles. Copper percentages and topological models are presented per each tile of all the active layers.

2.1. Two-dimensional composite models for the representation of each tile

If the tiling process is accurate enough, then the microstructure of each tile can be adequately represented by one of the following models: (a) "lines", (b) "vias" or (c) "web".

2.1.1. "Lines" model

Let (x_1, x_2) be the principal system of coordinates for a copper line-reinforced polymer matrix composite plate. Let x_1 be aligned with the copper lines direction (Fig. 4b). Then, from elasticity considerations, the effective properties of the composite in the principal coordinate system are [23]:

$$
\begin{aligned}
E_{11}^{\text{lines}} &= \phi_{\text{Cu}} E_{\text{Cu}} + \phi_{\text{res}} E_{\text{res}} \\
E_{22}^{\text{lines}} &= \frac{E_{\text{Cu}} E_{\text{res}}}{\phi_{\text{Cu}} E_{\text{res}} + \phi_{\text{res}} E_{\text{Cu}}} \\
G_{12}^{\text{lines}} &= \frac{G_{\text{Cu}} G_{\text{res}}}{\phi_{\text{Cu}} G_{\text{res}} + \phi_{\text{res}} G_{\text{Cu}}} \\
v_{12}^{\text{lines}} &= \phi_{\text{Cu}} v_{\text{Cu}} + \phi_{\text{res}} v_{\text{res}}
\end{aligned}
\tag{1}
$$

where ϕ is the volume fraction, E is the Young's modulus, G is the shear modulus and v is the Poisson's ratio (and the subscripts Cu and res refer to copper and resin, respectively). Analogously, the effective coefficients of thermal expansion are [23]:

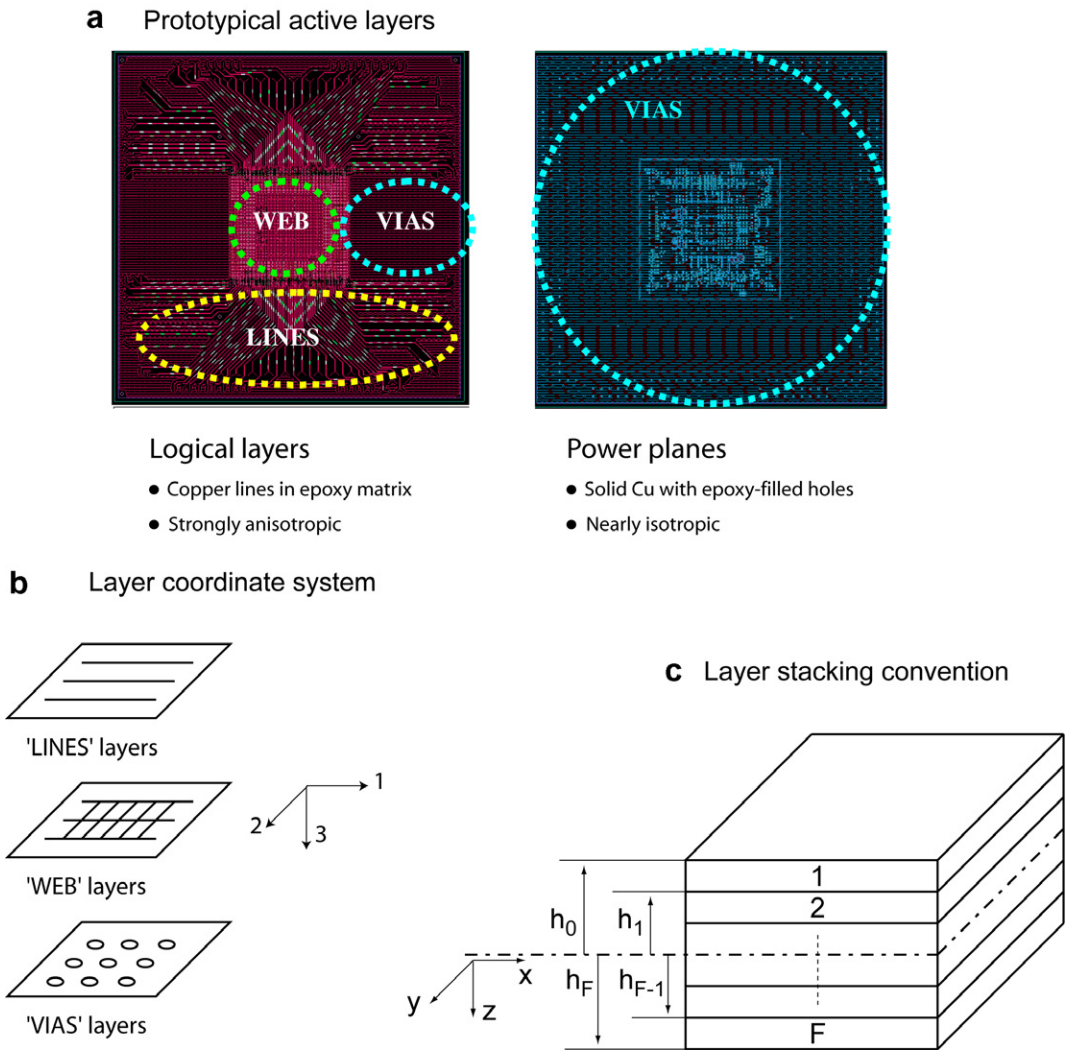

Fig. 4. (a) Drawings of two different active layers for a medium core thickness substrate. The modeling approaches for different areas are depicted. (b) Coordinate system relative to the microstructure of each modeled layer. (c) Layer stacking convention for the lamination process (from [23]).

$$\begin{aligned}\alpha_{11}^{\text{lines}} &= \frac{\phi_{\text{Cu}}E_{\text{Cu}}\alpha_{\text{Cu}} + \phi_{\text{res}}E_{\text{res}}\alpha_{\text{res}}}{\phi_{\text{Cu}}E_{\text{Cu}} + \phi_{\text{res}}E_{\text{res}}}\\ \alpha_{22}^{\text{lines}} &= (1+\nu_{\text{Cu}})\phi_{\text{Cu}}\alpha_{\text{Cu}} + (1+\nu_{\text{res}})\phi_{\text{res}}\alpha_{\text{res}}\\ &\quad - \alpha_{11}^{\text{lines}}(\phi_{\text{Cu}}\nu_{\text{Cu}} + \phi_{\text{res}}\nu_{\text{res}})\end{aligned} \tag{2}$$

where α_{Cu} and α_{res} are the coefficients of thermal expansion of copper and resin, respectively.

2.1.2. "Vias" model

In this model, we consider a copper plate with a number of holes (Fig. 4b). Notice that in actual substrates these holes (vias) consist of a copper clad filled with resin. For the sake of simplicity, we choose to ignore the contribution of the resin; given that its modulus (4 GPa) is much smaller than that of copper (115 GPa), this is not expected to introduce significant errors.

If the distribution of holes is isotropic and the volume fraction of holes (ϕ_{holes}) is quite small, then analytical solutions exist for the effective properties [24]:

$$\begin{aligned}\frac{E_{11}^{\text{vias}}}{E_{\text{Cu}}} &= \frac{E_{22}^{\text{vias}}}{E_{\text{Cu}}} = 1 - 3\phi_{\text{holes}} + \text{O}(\phi_{\text{holes}}^2)\\ \nu_{12}^{\text{vias}} &= \nu_{21}^{\text{vias}} = \nu_{\text{Cu}} + (1-3\nu_{\text{Cu}})\phi_{\text{holes}} + \text{O}(\phi_{\text{holes}}^2)\\ G_{12}^{\text{vias}} &= \frac{E_{11}^{\text{vias}}}{2(1+\nu_{12}^{\text{vias}})}\\ \alpha_{11}^{\text{vias}} &= \alpha_{22}^{\text{vias}} = \alpha_{\text{Cu}}\end{aligned} \tag{3}$$

Notice that (i) the resultant composite material is isotropic, as expected, and that (ii) this model is only accurate at first order in the volume fraction of holes. Notice also that a small fraction of holes has a large effect on the Young's modulus, but does not alter the coefficient of thermal expansion.

Although appealing for its simplicity, this model cannot adequately represent the actual 'vias' layer, given that in most substrates the density of holes often exceeds 20% and their distribution is not isotropic (most often, the holes are arranged in a square pattern, either at 0° or at 45° angle

with the substrate sides). To obtain a better representation for the effective properties, a number of finite elements simulations were run on a square pattern of holes, at various volume fractions ϕ_{holes}. As expected, the results agreed very well with the first-order analytical model at low ϕ_{holes}, but revealed a significant deviation at higher holes densities (Fig. 5). The finite elements results were fitted with 4th-order polynomial curves, in order to derive a working expression for the effective properties:

$$\begin{aligned}
\frac{E_{11}^{\text{vias}}}{E_{\text{Cu}}} &= \frac{E_{22}^{\text{vias}}}{E_{\text{Cu}}} = 0.998 - 3.220\phi_{\text{holes}} + 9.238\phi_{\text{holes}}^2 \\
&\quad - 18.037\phi_{\text{holes}}^3 + 13.630\phi_{\text{holes}}^4 \\
\frac{G_{11}^{\text{vias}}}{G_{\text{Cu}}} &= \frac{G_{22}^{\text{vias}}}{G_{\text{Cu}}} = 1.008 - 3.266\phi_{\text{holes}} + 1.420\phi_{\text{holes}}^2 \\
&\quad + 6.560\phi_{\text{holes}}^3 - 7.600\phi_{\text{holes}}^4 \\
v_{12}^{\text{vias}} &= v_{\text{Cu}} + 0.092\phi_{\text{holes}} - 1.838\phi_{\text{holes}}^2 \\
&\quad + 3.810\phi_{\text{holes}}^3 - 2.928\phi_{\text{holes}}^4 \\
\alpha_{11}^{\text{vias}} &= \alpha_{22}^{\text{vias}} \cong \alpha_{\text{Cu}}
\end{aligned} \tag{4}$$

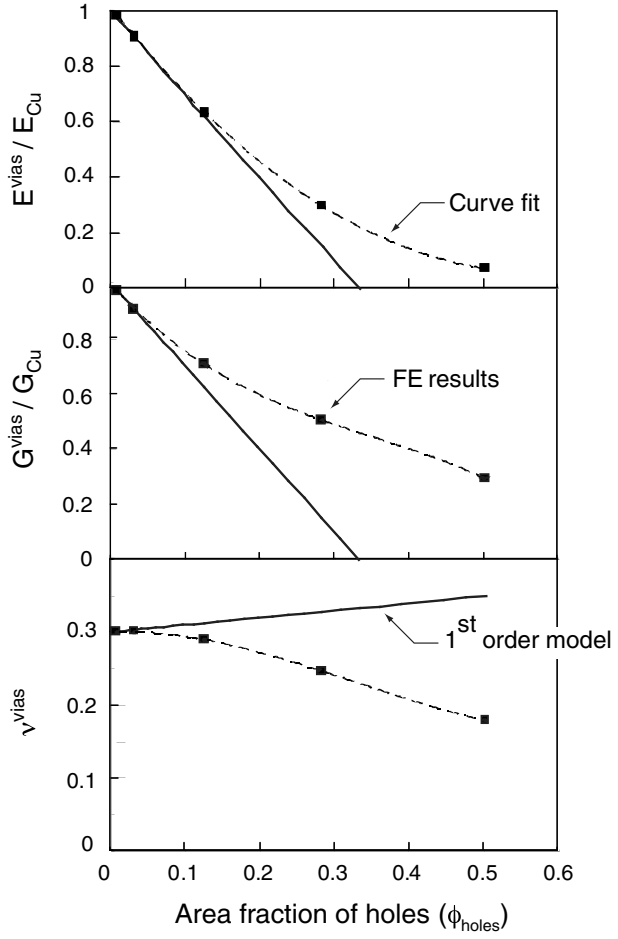

Fig. 5. Comparison between first-order analytical predictions for an isotropic distribution of holes (from [24]) and FE results for a square pattern of holes. The 4th-order polynomial fit (dashed curve) is used in the "vias" model. $v_{\text{Cu}} = 0.3$ has been used for the calculations leading to (c).

2.1.3. "Web" model

Under the chip footprint, typically there are copper lines running both along the top–bottom and the left–right directions. This kind of layer can be idealized as a superposition of two orthogonal 'lines' layers.

The stiffness matrix for an orthotropic material is given by [23]:

$$[Q] = \begin{bmatrix} E_x/J & v_{xy}E_y/J & 0 \\ v_{xy}E_y/J & E_y/J & 0 \\ 0 & 0 & G_{xy} \end{bmatrix} \tag{5}$$

where v_{xy} is the ratio of the contraction along the y direction to the extension along the $x$direction when a tensile stress is applied along the x direction, E_x and E_y are the Young's moduli in the two principal directions, G_{xy} is the shear modulus, and $J = 1 - v_{xy}v_{yx}$. Notice that the Poisson's ratios v_{xy} and v_{yx} must satisfy the condition $v_{xy}/E_x = v_{yx}/E_y$. If all the lines were aligned along the x directions, the stiffness matrix would be:

$$[Q]_0 = \begin{bmatrix} E_{11}^{\text{lines}}/J & v_{12}^{\text{lines}}E_{22}^{\text{lines}}/J & 0 \\ v_{12}^{\text{lines}}E_{22}^{\text{lines}}/J & E_{22}^{\text{lines}}/J & 0 \\ 0 & 0 & G_{12}^{\text{lines}} \end{bmatrix} \tag{6}$$

analogously, for the lines oriented along the y directions, we would have:

$$[Q]_{90} = \begin{bmatrix} E_{22}^{\text{lines}}/J & v_{12}^{\text{lines}}E_{22}^{\text{lines}}/J & 0 \\ v_{12}^{\text{lines}}E_{22}^{\text{lines}}/J & E_{11}^{\text{lines}}/J & 0 \\ 0 & 0 & G_{12}^{\text{lines}} \end{bmatrix} \tag{7}$$

The stiffness matrix for the "web" model will then be the average of the matrices relative to the 0° and 90° line orientations:

$$\begin{aligned}
[Q] &= \frac{[Q]_0 + [Q]_{90}}{2} \\
&= \begin{bmatrix} \left(E_{11}^{\text{lines}} + E_{22}^{\text{lines}}\right)/2J & v_{12}^{\text{lines}}E_{22}^{\text{lines}}/J & 0 \\ v_{12}^{\text{lines}}E_{22}^{\text{lines}}/J & \left(E_{11}^{\text{lines}} + E_{22}^{\text{lines}}\right)/2J & 0 \\ 0 & 0 & G_{12}^{\text{lines}} \end{bmatrix}
\end{aligned} \tag{8}$$

The effective properties can be easily derived by inverting this matrix. If $[S] = [Q]^{-1}$, then:

$$\begin{aligned}
E_{11}^{\text{web}} &= E_{22}^{\text{web}} = 1/S_{11} \\
G_{12}^{\text{web}} &= 1/S_{33} \\
v_{12}^{\text{web}} &= -S_{12}/S_{11}
\end{aligned} \tag{9}$$

The effective coefficients of thermal expansion can be derived using lamination theory (the details of the derivation are presented in the following section):

$$\begin{pmatrix} \alpha_{11}^{\text{web}} \\ \alpha_{22}^{\text{web}} \\ \alpha_{12}^{\text{web}} \end{pmatrix} = [S] \cdot \left(\frac{1}{2}[Q]_0 \cdot \begin{pmatrix} \alpha_{11}^{\text{lines}} \\ \alpha_{22}^{\text{lines}} \\ 0 \end{pmatrix} + \frac{1}{2}[Q]_{90} \cdot \begin{pmatrix} \alpha_{22}^{\text{lines}} \\ \alpha_{11}^{\text{lines}} \\ 0 \end{pmatrix} \right) \tag{10}$$

The accuracy of this model was verified against a set of selected finite elements calculations. In all calculations, a unit cell of the web layer was modeled, with periodic boundary conditions. Both Copper and Resin regions were meshed (see Table 1 for the materials properties; the resin used in the medium core substrates was used). A large range of copper content was explored (17.4–55.6%). The results (Fig. 6) clearly show that the effective Young's modulus and coefficient of thermal expansion are captured very accurately by the 'web' model. The agreement is less satisfactory for the effective shear modulus and Poisson's ratio. Since the Young's modulus and the CTE have the larger effect on the overall effective properties of the substrate, these discrepancies are ignored. Also notice that numerical results obtained without meshing the resin region show substantial discrepancy with fully meshed calculations, revealing that in the 'web' configuration, the resin has a substantial role in defining the effective properties; as a result, fitting copper-only numerical results would result in worse accuracy than using the analytical model. Fitting

Table 1
Materials properties used in all the calculations

	E (GPa)	ν	α (10^{-6}/K)
Copper	115	0.3	17
Silicon	130	0.3	2.5
Resin			
Thick core	3	0.41	95
Medium core	4	0.3	95
Coreless	4	0.3	46
Solder mask			
Thick core	2.6	0.31	55
Medium core	2.5	0.3	90
Coreless	2.6	0.3	46
Core			
Thick core	23.5	0.18	15
Medium core	27	0.3	14

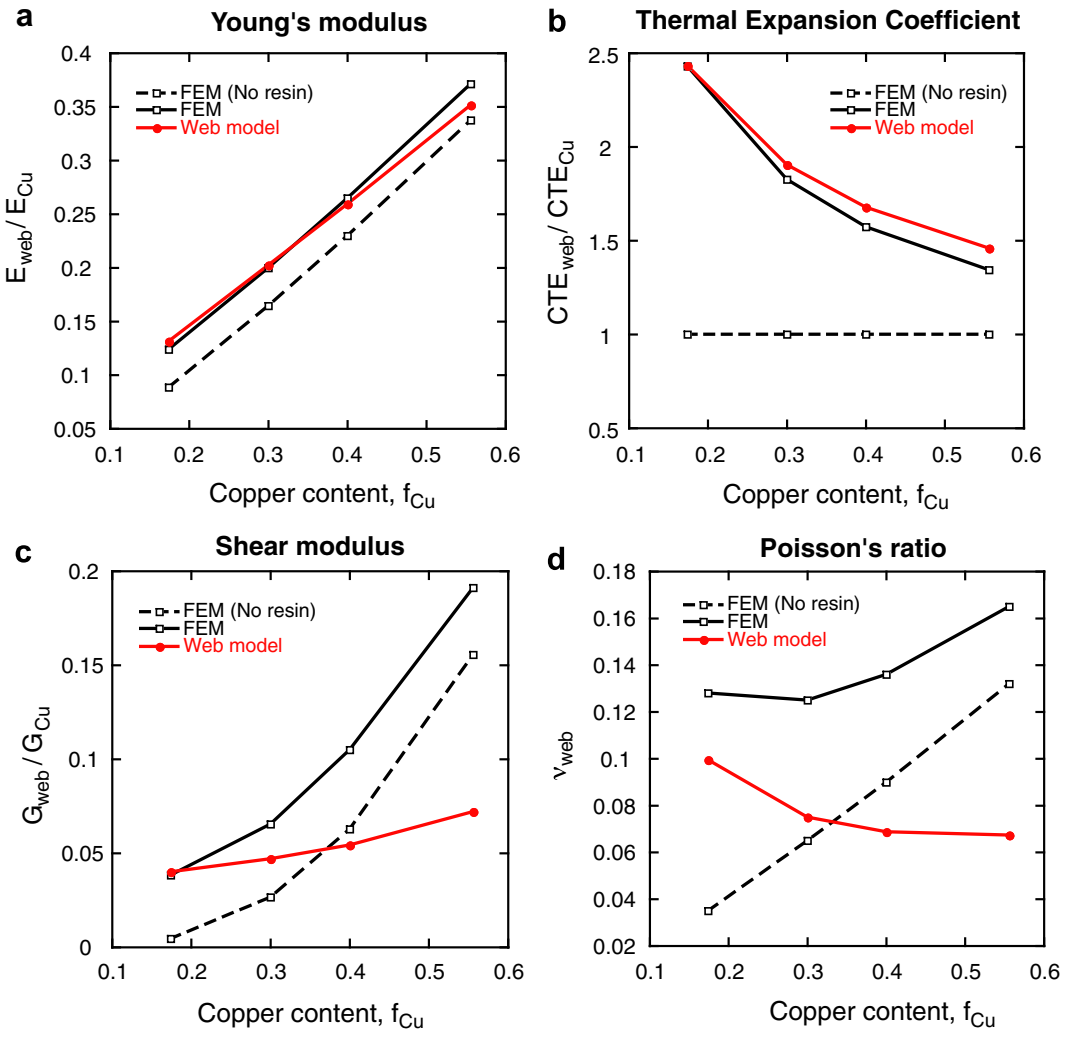

Fig. 6. Comparison between analytical predictions and finite elements calculations for the effective properties of the 'web' model: (a) Young's modulus; (b) Coefficient of thermal expansion; (c) Shear modulus; (d) Poisson's ratio. Notice that the fully-meshed numerical solution agrees very well with the model for Young's modulus and CTE (the most important properties); the agreement is less satisfactory for shear modulus and Poisson's ratio. Interestingly, the resin has a significant effect on the effective properties (copper-only solutions cannot even capture the right trends). The materials properties used in the calculations are reported in Table 1 (the resin of the medium core substrate was used).

the fully-meshed finite elements results would yield results that are dependent on the materials properties of the resin used; as these properties can exhibit large variations (see Table 1), the results would loose in generality. All things considered, the analytical 'web' model provides the most general results with a very satisfactory accuracy, and we decide to use it with no fitting from the finite element results.

2.2. Lamination approach

Using the method presented in Section 2.1, the orthotropic thermo-elastic properties of every tile in each layer were derived. The next step consists of assembling the layers together and computing the effective properties of the resulting laminated tiles. Classic lamination theory is used [23], thus neglecting the shear compliance of the laminate; given that the aspect ratio of the substrate (side/thickness) is typically large (>50), this assumption is not believed to affect the results significantly. In classic plate theory, the stiffness of a plate is defined as the matrix that relates the normal and shear forces per unit width (N_x, N_y, N_{xy}) and the bending and twisting moments per unit width (M_x, M_y, M_{xy}) to the normal and shear strains of the neutral axis $(\varepsilon_x^0, \varepsilon_y^0, \gamma_{xy}^0)$ and the bending and twisting curvatures $(\kappa_x, \kappa_y, \kappa_{xy})$. The total elastic strains of the plate can be expressed as: $\varepsilon_x = \varepsilon_x^0 + \kappa_x z$ (and analogously for the other components), where z is the distance from the neutral axis.

For a homogeneous plate, in a linear theory, the application of normal and shear forces produces no curvature, and similarly the application of bending and twisting moments will produce no normal or shear strain at the neutral axis. Analogously, a change in temperature will induce uniform strains only, and no thermal curvatures are generated. Under these conditions, the complete thermo-elastic response of the plate (neglecting transverse shear compliance) can be expressed as:

$$\begin{bmatrix}[N]\\ [M]\end{bmatrix} = \begin{bmatrix}[A] & 0\\ 0 & [D]\end{bmatrix}\begin{bmatrix}[\varepsilon^0]\\ [\kappa]\end{bmatrix} - \begin{bmatrix}[N^{\mathrm{T}}]\\ [0]\end{bmatrix} \tag{11}$$

where the matrix $[A]$ expresses the stretching/shearing stiffness, the matrix $[D]$ expresses the bending/twisting stiffness of the plate, and $[N^{\mathrm{T}}]$ is the thermal force. If the material of the plate is characterized by a stiffness matrix $[Q]$ and coefficients of thermal expansion $[\alpha_x, \alpha_y, 0]^{\mathrm{T}}$, where

$$\begin{pmatrix}\sigma_x\\ \sigma_y\\ \tau_{xy}\end{pmatrix} = [Q]\left\{\begin{pmatrix}\varepsilon_x\\ \varepsilon_y\\ \gamma_{xy}\end{pmatrix} - \begin{pmatrix}\alpha_x\\ \alpha_y\\ 0\end{pmatrix}\Delta T\right\} \tag{12}$$

It then follows that $[A] = h[Q]$, $[B] = \frac{h^3}{12}[Q]$, and $[N^{\mathrm{T}}] = h[Q][\alpha]\Delta T$, with h being the plate thickness.[1]

For laminated plates, it can be shown that the matrices $[A]$ and $[D]$ and the vector $[N^{\mathrm{T}}]$ can be obtained via an assembly process involving the effective matrices $[Q]$ of each layer (all expressed in the same reference system as the overall plate), the layer thicknesses and the lay-up arrangement (i.e. the order of stacking). If the laminate is not symmetric with respect to its mid-plane, then a new matrix $[B]$ will arise, relating forces to curvatures and moments to strains of the neutral axis; similarly, a thermal moment $[M^{\mathrm{T}}]$ will appear.

The most general thermo-elastic response of a laminated plate can then be expressed as

$$\begin{bmatrix}[N]\\ [M]\end{bmatrix} = \begin{bmatrix}[A] & [B]\\ [B] & [D]\end{bmatrix}\begin{bmatrix}[\varepsilon^0]\\ [\kappa]\end{bmatrix} - \begin{bmatrix}[N^{\mathrm{T}}]\\ [M^{\mathrm{T}}]\end{bmatrix} \tag{13}$$

where the $[A]$, $[B]$ and $[D]$ matrix are obtained as

$$\begin{aligned}[A] &= \sum_{f=1}^{F}[Q]_f(h_f - h_{f-1})\\ [B] &= \frac{1}{2}\sum_{f=1}^{F}[Q]_f(h_f^2 - h_{f-1}^2)\\ [D] &= \frac{1}{3}\sum_{f=1}^{F}[Q]_f(h_f^3 - h_{f-1}^3)\end{aligned} \tag{14}$$

and the thermal loads are given by:

$$\begin{aligned}[N^{\mathrm{T}}] &= \Delta T\cdot\sum_{f=1}^{F}[Q]_f\cdot[\alpha]_f(h_f - h_{f-1})\\ [M^{\mathrm{T}}] &= \Delta T\cdot\frac{1}{2}\sum_{f=1}^{F}[Q]_f\cdot[\alpha]_f(h_f^2 - h_{f-1}^2)\end{aligned} \tag{15}$$

In these expressions, F is the total number of layers, and h_f is the vertical coordinate of the fth layer, measured from the mid-plane of the laminated plate (which might not coincide with its neutral axis of bending) – see Fig. 4c. Notice that while the matrix $[A]$ and the vector $[N^{\mathrm{T}}]$ are unaffected by the layer arrangement (they are mere averages of the contributions of each layer weighed on the layer thickness), the matrices $[B]$ and $[D]$ and the vector $[M^{\mathrm{T}}]$ weigh the external layers more than the internal ones. As a consequence, a laminated plate will have in general different stretching and bending responses, depending on the layer arrangement.

Before the $[A]$, $[B]$ and $[D]$ matrices of the laminated tile can be assembled, the stiffness matrices and the coefficients of thermal expansion of each layer must be rotated (whenever necessary) so that they all refer to the global coordinate system (x, y) (Fig. 4c). This can be readily accomplished as

[1] The shear strain γ_{xy} is the so-called engineering strain, which is defined as twice the tensor strain ε_{xy}.

$$[Q]_f^{(x,y)} = [T]^{-1}[Q]_f^{(1,2)}[R][T][R]^{-1}$$
$$[\alpha]_f^{(x,y)} = [T]^{-1}[\alpha]_f^{(1,2)} \tag{16}$$

where the matrix $[T]$ is the rotation matrix, expressed by:

$$[T] = \begin{bmatrix} \cos^2\theta & \sin^2\theta & 2\sin\theta\cos\theta \\ \sin^2\theta & \cos^2\theta & -2\sin\theta\cos\theta \\ -\sin\theta\cos\theta & \sin\theta\cos\theta & \cos^2\theta - \sin^2\theta \end{bmatrix} \tag{17}$$

(the angle θ measures the *counterclockwise* rotation necessary to bring the axis x to coincide with the axis x_1).[2]

Once the $[ABD]$ matrix is assembled, it can be inverted to obtain:

$$\begin{bmatrix} [\varepsilon^0] \\ [\kappa] \end{bmatrix} = \begin{bmatrix} [a] & [b] \\ [h] & [d] \end{bmatrix} \begin{bmatrix} [N] \\ [M] \end{bmatrix} + \begin{bmatrix} [\varepsilon_0^T] \\ [\kappa^T] \end{bmatrix} \tag{18}$$

where the thermal strains and curvatures are given by:

$$\begin{bmatrix} [\varepsilon_0^T] \\ [\kappa^T] \end{bmatrix} = \begin{bmatrix} [a] & [b] \\ [h] & [d] \end{bmatrix} \begin{bmatrix} [N^T] \\ [M^T] \end{bmatrix} \tag{19}$$

This completes the thermo-elastic characterization of the substrate.

2.3. Effective properties of the substrate

The effective thermo-elastic properties of the laminated tile can be immediately derived from the $[abhd]$ matrix (Eq. (18)) and the thermal strains and curvatures (Eq. (19)). For the effective homogeneous plate, $[A] = [Q]h$ and $[D] = [Q]h^3/12$, resulting in the following relations:

- Stretching moduli

$$E_x^{\text{laminate}} = \frac{1}{a_{11}h} \quad E_y^{\text{laminate}} = \frac{1}{a_{22}h}$$
$$\nu_{xy}^{\text{laminate}} = -\frac{a_{12}}{a_{11}} \quad G_{xy}^{\text{laminate}} = \frac{1}{a_{33}h} \tag{20}$$

- Bending moduli

$$EB_x^{\text{laminate}} = \frac{12}{d_{11}h^3} \quad EB_y^{\text{laminate}} = \frac{12}{d_{22}h^3} \tag{21}$$

- Coefficients of thermal expansion

$$\alpha_x^{\text{laminate}} = \frac{\varepsilon_{01}^T}{\Delta T} \quad \alpha_y^{\text{laminate}} = \frac{\varepsilon_{02}^T}{\Delta T} \quad \alpha_{xy}^{\text{laminate}} = \frac{\varepsilon_{03}^T}{\Delta T} \tag{22}$$

[2] The matrix $[R]$ is simply given by: $[R] = \begin{bmatrix} 1 & 0 & 0 \\ 0 & 1 & 0 \\ 0 & 0 & 2 \end{bmatrix}$. Its introduction is only necessary because the shear strain γ_{xy} used in all our analyses is the engineering strain, which is twice as large as the tensor strain ε_{xy} (hence the factor 2 in the $[R]$ matrix).

3. Experimental verification

Bending moduli and coefficients of thermal expansion were measured in various regions of three different substrates of commercial interest, mainly differing for their core thickness (926 μm, 400 μm and coreless, respectively). All substrates measured 42 mm × 42 mm. Test specimens were extracted from the substrates using a diamond dicing saw (Fig. 7). To minimize the influence of moisture absorption, all the specimens were baked at 130 °C for 8 h and stored in a dry atmosphere prior to the measurements.

The bending moduli were measured using a Dynamic Mechanical Analyzer (TA Instruments DMA 2980). A miniature three-point bending fixture was used with a 10 mm bend span. The experiments were performed over a temperature range of −40 to 225 °C. Each result was averaged on a minimum of two measurements. A Thermal Mechanical Analyzer (TMA) was used to extract the CTE values. A quartz probe was used in the compression mode. The square specimens were placed vertically between this probe and the quartz tube. For the thinner specimens a quartz holder was utilized to hold the specimens vertical. Measurements were made both along the x and y directions; each result was averaged on a minimum of two experiments. The bending modulus and CTE at 25 °C (room temperature) for each sample were compared with the predicted values in the same region (the material properties used for modeling are reported in Table 1). Fig. 8 presents the agreement between model and experiments. Notice that most of the experimental values fall within 10% of the predicted values. Fig. 9 presents the results in more detail for the medium core thickness substrate, indicating the position of the specimen within the substrate.

Although in general satisfactory, the agreement is not always excellent. The disagreement is attributed to three factors: (a) the averaging process described in Section 2 was performed on tiles slightly larger than those used for the measurements; (b) organic substrates are known to experience aging, which might alter the properties of its constituents; (c) the manufacturing processes are not exactly reproducible, and some variation in the properties was observed on nominally identical samples; for the case of the medium core substrate, variations in the bending modulus exceeded 15% on some locations, whereas CTE measurements were more reproducible. All these issues are currently being investigated. Notice that the spatial variation of the CTE is not very significant for the medium core substrate – Fig. 9 (typically, variations are not larger than 1×10^{-6}/K).

4. Model results

The three substrates studied were divided in nine tiles and the effective thermo-elastic properties of each tile were calculated (as per Eqs. (20)–(22)). The results are presented in Fig. 10. The shaded areas are significantly stiffer than any other part of the substrate, whereas the coefficients

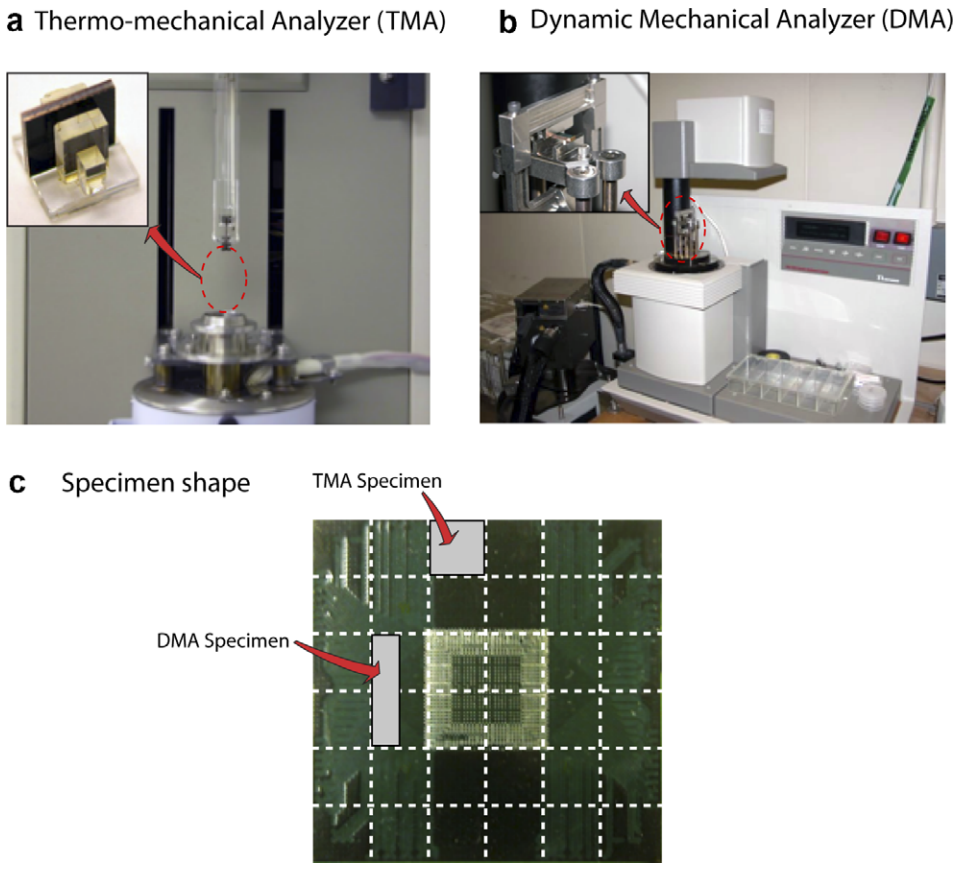

Fig. 7. (a) Thermo-mechanical analyzer (TMA) used to measure the thermal expansion coefficients. The inset shows the sample holder. (b) Dynamic mechanical analyzer (DMA) used to measure the elastic moduli. The inset shows the three-point-bending fixture. (c) Schematic of the specimen shape and size relative to the whole substrate.

of thermal expansion are fairly uniform. These findings highlight optimal regions for the placement for various elements on the substrate, including capacitors (IDC) and resistors: since stiffer substrates in general translate in higher stresses on the capacitor joints under thermal loads, capacitors on stiffer areas should be avoided whenever possible. It is important to notice that this conclusion might not apply under mechanical loads, where large substrate stiffness translates in lower strains; multi-objective optimization strategies are needed to extract the optimal substrate stiffness under multiple load scenarios.

The values obtained for each laminated tile can be averaged to express the overall effective properties of the substrate. The averaged results for the investigated substrates are presented in Table 2. For the medium core substrate, the effective properties were calculated by starting from the bare core, and successively adding two layers at a time (one on each side). Fig. 11 shows the variation of the effective elastic moduli and CTEs (averaged over all the tiles) as all the layers are progressively added. Notice that the bending modulus decreases as more layers are added: this is due to the fact that the core is relatively stiff compared to the external layers. Obviously the stiffness of the laminate (force/moment necessary to achieve a given deformation/curvature) is monotonically increasing with the number of layers. Notice that the third active layers on top and bottom sides of the core (corresponding to layers FC1 and BC1 in Fig. 3) are the most influential in raising the bending stiffness and limiting the CTE: this is due to their particularly large copper content (Fig. 3) as well as their location far from the neutral axis of the laminate. For situations in which it might be desirable to alter the properties of the substrate to achieve some objective (e.g. reduce warp, or stresses in a capacitor), this information reveals on which layers it is more effective to focus.

5. Application of the model to finite elements (FE) studies

In the previous section, the model has been used to extract a set of effective thermo-elastic properties in selected regions of substrates of commercial interest. When finite elements (FE) models of more complex structures (e.g. flip-chip packages with capacitors, resistors, and thermal solutions) are needed, it is convenient to represent the substrate as a solid object, characterized by an anisotropic compliance matrix and CTEs. Referring again to Fig. 2, several modeling options are available. In the (x, y) plane, any number of tiles can be used, and the considerations discussed before apply: increasing the number of tiles involves

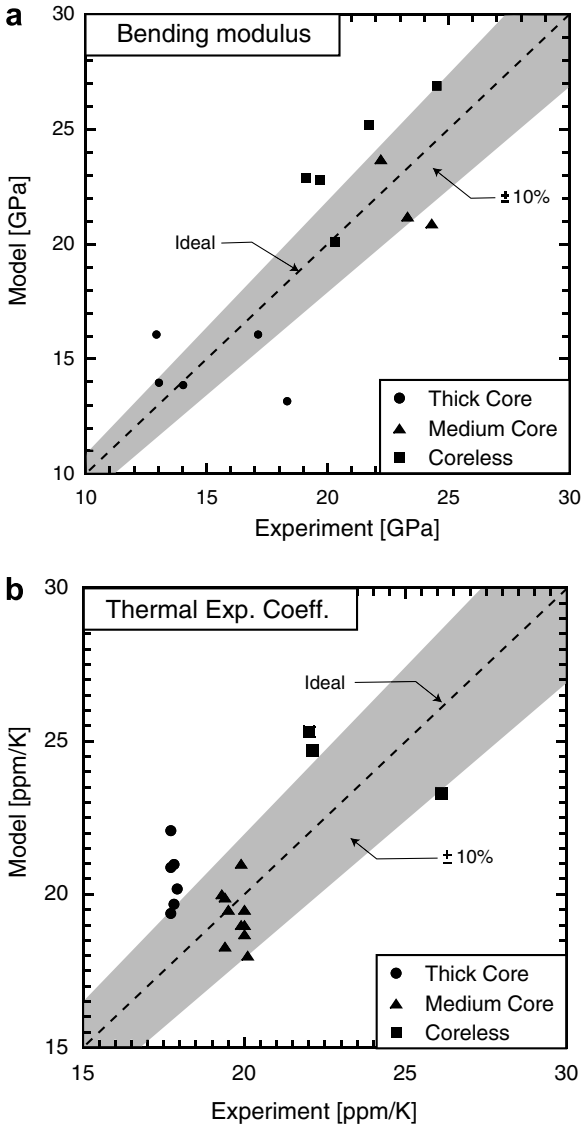

Fig. 8. Cross-plot of measured and calculated values for (a) bending modulus and (b) thermal expansion coefficient for the three substrates under investigation. Notice that in most cases, the model agrees with the experimental results within 10%.

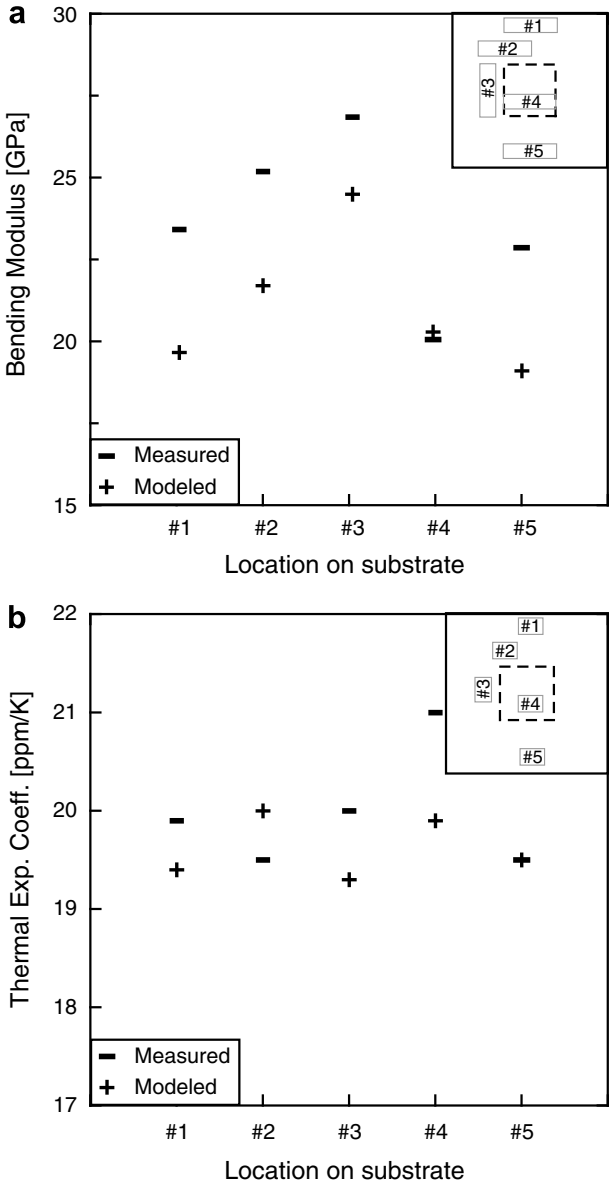

Fig. 9. Comparison of experimental and predicted values for (a) the bending modulus and (b) the coefficient of thermal expansion for the medium-core substrate. The insets show the position of the various samples within the substrate.

more time in extracting the properties and a slightly longer FE execution time (due to the increasing number of tied regions). In the z direction, the situation is subtler: if the [*abhd*] matrix of the composite plate (encompassing all the layers) is used to extract effective thermo-elastic properties, then the difference between the stretching and bending response is inevitably lost (in particular, no warp can be predicted upon heating or cooling). To address this problem, we suggest modeling each tile as a stacking of three effective layers (typically the core and two effective active layers), modeled as solid objects glued to each other. The anisotropic thermo-elastic properties of each effective layer (in each tile) can be derived for from the associated [*abhd*] matrix (which is obtained as per Eqs. (18) and (19), by including the desired number of layers). Since the [*abhd*] description of a plate is a two-dimensional description, it can provide no information on the z-components of the effective compliance matrix: Appendix 1 presents an approximate model to estimate these components.

For situations in which a one-layer model has to be used (e.g. to decrease the computation time), then the compliance matrix should be extracted from the bending component of the [*abhd*] matrix (i.e. the [*d*] matrix): this is motivated by the observation that in typical service conditions the substrate is primarily loaded in bending (rather than in-plane stretching). Conversely, if three or more effective layers are used, then the bending behavior is already captured by the topology of the solid object, and the stretching component of the [*abhd*] matrix (i.e. the [*a*] matrix) provides a more realistic representation.

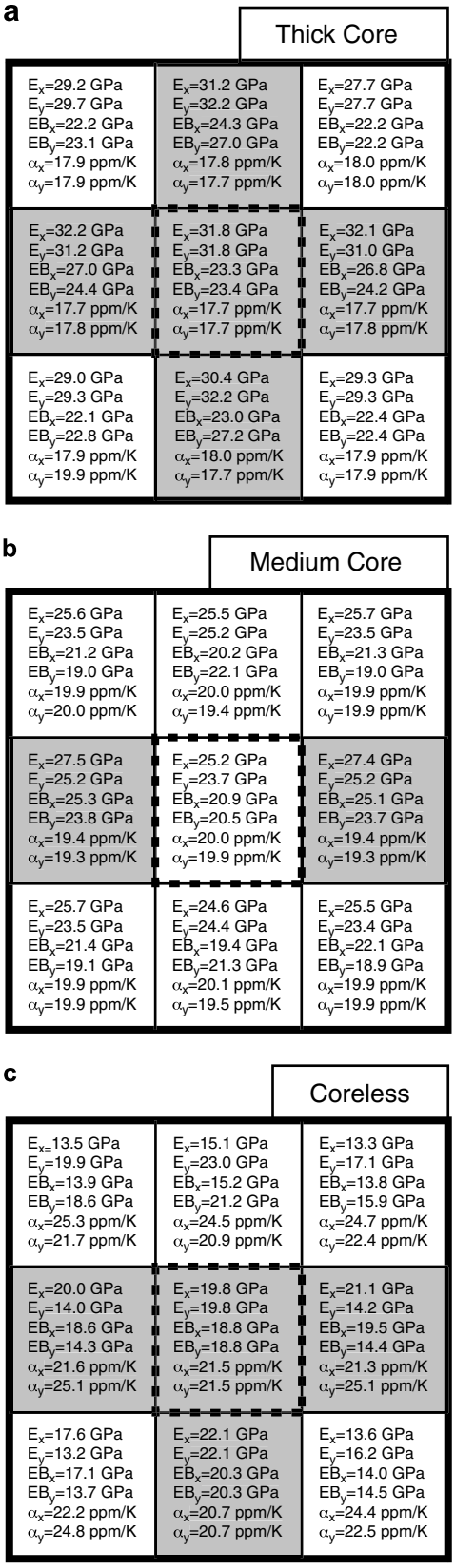

Fig. 10. In-plane properties distribution for (a) thick core, (b) medium core and (c) coreless substrates. The shaded areas represent the regions where the Young's modulus is significantly higher and the CTE is significantly lower than anywhere else in the substrate. Values for the elastic moduli are in GPa, values for CTE are in ppm/K.

The thermo-elastic behavior of a three-dimensional, fully anisotropic solid is characterized by 21 elastic constants and three coefficients of thermal expansion:

$$\begin{Bmatrix}\varepsilon_1\\ \varepsilon_2\\ \varepsilon_3\\ \gamma_{23}\\ \gamma_{31}\\ \gamma_{12}\end{Bmatrix}=\begin{bmatrix}C_{11} & C_{12} & C_{13} & C_{14} & C_{15} & C_{16}\\ & C_{22} & C_{23} & C_{24} & C_{25} & C_{26}\\ & & C_{33} & C_{34} & C_{35} & C_{36}\\ & & & C_{44} & C_{45} & C_{46}\\ & & & & C_{55} & C_{56}\\ & & & & & C_{66}\end{bmatrix}\begin{Bmatrix}\sigma_1\\ \sigma_2\\ \sigma_3\\ \tau_{23}\\ \tau_{31}\\ \tau_{12}\end{Bmatrix}+\begin{Bmatrix}\alpha_1\\ \alpha_2\\ \alpha_3\\ 0\\ 0\\ 0\end{Bmatrix}\Delta T \tag{23}$$

where the compliance matrix $[C]$ is symmetric.[3] Its in-plane components can be extracted by the [*abhd*] matrix (Eqs. (18) and (19)) as follows:

1. *Derivation from the bending component of the [abhd] matrix*

$$C_{11}=\frac{h^3}{12}d_{11}\quad C_{12}=\frac{h^3}{12}d_{12}\quad C_{22}=\frac{h^3}{12}d_{22}\quad C_{16}=\frac{h^3}{12}d_{13}$$

$$C_{26}=\frac{h^3}{12}d_{23}\quad C_{66}=\frac{h^3}{12}d_{33}$$

$$C_{13}=-v_{13}/E_1=-v_{13}C_{11}\quad C_{23}=-v_{23}/E_2=-v_{23}C_{22}$$

$$C_{33}=1/E_3\quad C_{44}=1/G_{23}\quad C_{55}=1/G_{31}$$

$$C_{14}=C_{15}=C_{24}=C_{25}=C_{34}=C_{35}=C_{36}=Q_{45}=Q_{46}=Q_{56}\approx 0 \tag{24}$$

2. *Derivation from the stretching component of the [abhd] matrix*

$$C_{11}=ha_{11}\quad C_{12}=ha_{12}\quad C_{22}=ha_{22}\quad C_{16}=ha_{13}\quad C_{26}=ha_{23}$$

$$C_{66}=ha_{33}$$

$$C_{13}=-v_{13}/E_1=-v_{13}C_{11}\quad C_{23}=-v_{23}/E_2=-v_{23}C_{22}$$

$$C_{33}=1/E_3\quad C_{44}=1/G_{23}\quad C_{55}=1/G_{31}$$

$$C_{14}=C_{15}=C_{24}=C_{25}=C_{34}=C_{35}=C_{36}=Q_{45}=Q_{46}=Q_{56}\approx 0 \tag{25}$$

For both cases, the coefficients of thermal expansion are given by Eq. (22), and the out-of-plane components $(v_{13}, v_{23}, E_3, G_{23}, G_{31}, \alpha_3)$ are provided in Appendix 1.

In Eqs. (24) and (25), h is the thickness of the effective layer (e.g. the cumulative thickness of all active layers, resin and solder mask above the core, if a three-layer model is

[3] Notice that this notation is not the same used by the finite element code ANSYS™. ANSYS™ defines the shear stresses in the stress vector in the following order: τ_{12}, τ_{13}, τ_{23} (and analogously for the strains). Care should be taken to modify the indices of the compliance matrix, when using ANSYS™.

Table 2
Average properties for the analyzed substrates

Substrate	E_x (GPa)	E_y (GPa)	EB_x (GPa)	EB_y (GPa)	α_x (10^{-6}/K)	α_y (10^{-6}/K)
Thick core	30.3	30.5	23.7	24.1	17.8	18.0
Medium core	25.9	24.2	21.9	20.8	19.8	19.7
Coreless	17.3	17.7	16.8	16.9	22.9	22.7

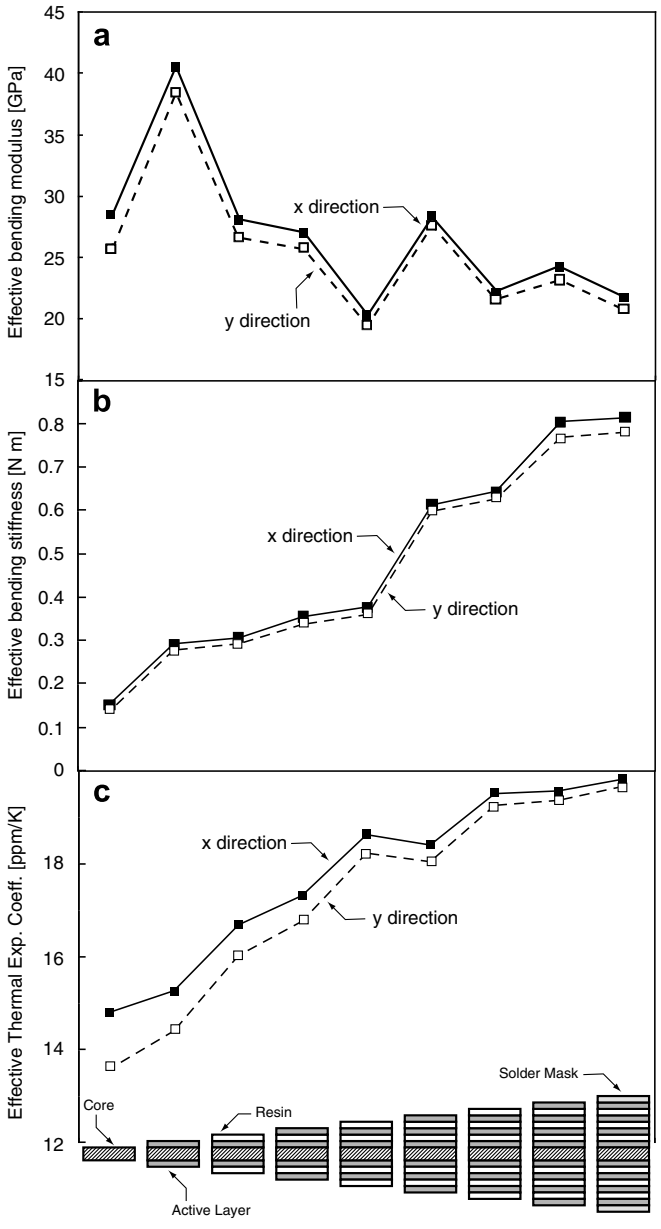

Fig. 11. Contribution of each layer to the overall effective properties for the medium-core substrate presented in Fig. 3: (a) bending modulus, (b) bending stiffness and (c) coefficient of thermal expansion. For each layer, the properties were averaged over the nine tiles.

used). Notice that some terms have been assumed equal to 0 in Eqs. (24) and (25) (exact only for orthotropic materials). Given that each tile is typically not too far from orthotropic, this approximation is believed to be adequate.

To explore the effect of these different modeling strategies, a silicon die/underfill/substrate assembly was modeled using the commercial finite element code ANSYS™. The substrate measured 42 mm × 42 mm, with a 15 mm × 15 mm Silicon die at the center. Fig. 12 presents the assembly warp resulting from a 180 °C temperature drop (representative of a *deep thermal cycle*, DTC). Three different modeling schemes were used for the medium core substrate:

1. *single layer, single tile* (Fig. 12a): this is the simplest and most economical representation. The substrate is modeled using solid shell elements with anisotropic elastic properties: the 21 compliance components were obtained as per Eq. (24), using the bending component of the [*abhd*] matrix. The [*abhd*] matrix was obtained by averaging each component over the 9 tiles.
2. *three layers, single tile* (Fig. 12b): unlike case 1, three effective layers of the substrate are modeled as separate regions, with different sets of properties. The central layer is modeled as an orthotropic material with the properties of the core (Table 1), whereas the top and bottom layers are an effective representation of the laminates above and below the core. For these two layers, the anisotropic properties are obtained as per Eq. (25).
3. *three layers, nine tiles* (Fig. 12c): this is the same as case 2, except that now the finite element model contains one region for the core and 18 effective regions for the top and bottom layers. The stretching component of the [*abhd*] matrix was used for all the properties.

The difference between a one-layer and a three-layer model is evident in comparing Fig. 12a and b. For the medium core substrate used in these analyses, the asymmetry of the substrate was such that its self-warp wanted to contrast that of the substrate. The result is that a one-layer model (resulting in no self-warp) overestimates the overall package warp by almost 20%. Notice that at the chip corner, the warp is rather insensitive to the model used. The assembly modeled in Fig. 12c exhibits significant anisotropy, resulting in the four corners of the substrate experiencing significantly different warps. This clearly suggests that tiling should always be implemented (we suggest a minimum of nine tiles for an adequate representation).

All these conclusions are clearly highlighted in Fig. 13, which superimposes warp profiles (along a diagonal) for the different calculations.

It is worth mentioning that all the FE simulations used materials properties evaluated at 25 °C. Although the moduli and CTE of copper do not vary much over the −25 to 155 °C temperature range, the same is not true for the resin (which undergoes glass transition at around 125 °C). Future analyses will make use of temperature-dependent properties for the resin, which can be easily incorporated in the model.

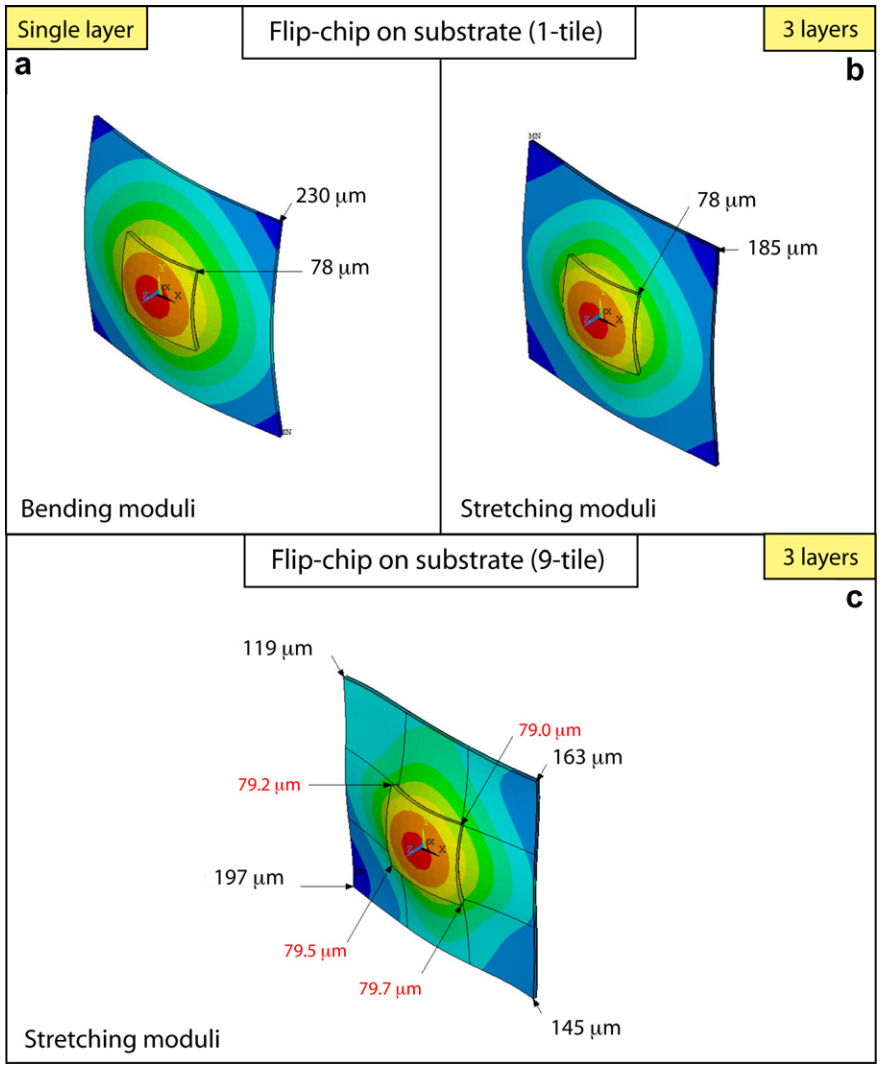

Fig. 12. Flip-chip package warp upon cooling for a 180 °C temperature drop (representative of a deep thermal cycle (DTC)). Different modeling approaches are illustrated, and the results compared. (a) Modeling the substrate as a single effective layer does not account for substrate self-warp, and in this case results in overestimation of the warp at the substrate corner. This problem is resolved by using three layers to model the substrate (b). Notice that warp at the chip corner is not sensitive to these modeling differences. (c) A three-layer, nine-tile model allows the significant anisotropy of the substrate to be captured.

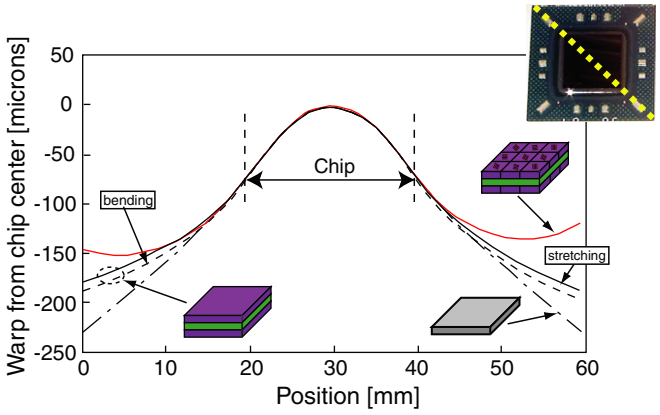

Fig. 13. Flip-chip package warp profiles upon cooling for a 180 °C temperature drop. Accounting for heterogeneity (red curve) has a significant effect on warp estimates. (For interpretation of the references to colour in this figure legend, the reader is referred to the web version of this article.)

6. Conclusions

This work presents a novel thermo-mechanical model of organic substrates, with the main attribute of allowing for various degrees of accuracy and complexity.

The substrate is initially divided in tiles in the (x, y) plane; the tiles should be sufficiently numerous to guarantee that each layer in each tile possesses a fairly uniform copper content and arrangement. Three different composite materials models are presented, and it is observed that sufficiently small regions in each layer can always be adequately represented by one of these models. Classical laminated plate theory is then used to assemble all the layers and derive the $[ABD]$ matrix of each tile.

A series of experiments were performed on various regions of three substrates of interest (mainly differing in core thickness), to measure the bending modulus and the

coefficient of thermal expansion. Experimental results typically agree within 10–15% with the model prediction.

Application of the model to the three aforementioned substrates revealed substantial in-plane elastic heterogeneity, whereas the coefficients of thermal expansion showed less significant variation. The effect of each layer on bending modulus and CTE was also presented; modification of the average properties of the substrate (e.g. to minimize thermal mismatch) should target the most influential layers. In general, we envision using the model presented in this paper in two different forms.

(i) For analytical calculations (e.g. to estimate C4 fatigue life, or stresses and strains at the substrate/underfill interface), the entire substrate can be represented as a simple orthotropic and homogeneous solid: the model provides the necessary properties by means of a simple averaging process.
(ii) In other situations (and they are the majority), the problem to be tackled is so formidable to exclude the possibility of a realistic analytical representation. In this case, finite elements (FE) modeling often emerge as the only viable approach. The model presented in this paper is used to extract effective properties for various regions of the substrate (each modeled as an anisotropic solid), with a number of effective layers and tiles appropriate for the accuracy required. This permits an economical but accurate FE representation of the substrate, which can then be used to model complex assemblies, possibly incorporating underfill, chip, and possibly stiffeners, caps, capacitors, etc.

Current improvements to the model include the introduction of temperature dependence on materials properties. Among the materials involved, the resin is by far the most temperature dependent. During DTC, the resin undergoes a glass transition at around 125 °C; if the resin modulus and CTE are known as a function of temperature, the model can be swept at different temperatures, and more realistic temperature-dependent sets of properties can be used in further FE analyses. For the sake of simplicity, the shear deformation of the layers (particularly the resin planes) was neglected in the present model; this assumption is valid at low temperatures, but becomes inappropriate as the glass transition temperature of the resin is approached. Work is under-way to address this deficiency. Finally, a critical problem in the characterization of organic substrates is failure analysis. Predicting and preventing the occurrence of failure necessitate two ingredients: accurate stress and/or strain estimates and suitable failure criteria. The model presented in this paper can offer some insights on the average stresses in all the layers, as well as the shear stresses at the interfaces. This information can be used to prevent the occurrence of delamination. It is important to notice, though, that a number of failure mechanisms are driven by highly localized stress states, that cannot be captured by a global model. Global/local modeling schemes [22] are needed for this task.

Finally, we emphasize that all the modeling approaches presented in this paper have been coded in an automatic fashion; the only procedure that is left to the operator is the decision of the desired number of tiles and the association of each tile to the appropriate composite material model.

Appendix 1. Out-of-plane properties

As long as the aspect ratio of a plate (side/thickness) is large enough, its elastic response to bending and transverse shear loads (including the out-of-plane deformation) is dominated by in-plane elastic properties. This implies that a number of approximations can be adopted in estimating the out-of-plane components of the compliance matrix (Eq. (23)) of each laminated tile without affecting the results significantly. In particular, it is convenient to assume that every layer in each tile is orthotropic, and that its principal axes are aligned with the global (x, y) axes. The compliance matrix for an orthotropic material is given by [25]:

$$C = \begin{bmatrix} 1/E_x & -\nu_{xy}/E_x & -\nu_{xz}/E_x & 0 & 0 & 0 \\ -\nu_{xy}/E_x & 1/E_y & -\nu_{yz}/E_y & 0 & 0 & 0 \\ -\nu_{xz}/E_x & -\nu_{yz}/E_y & 1/E_z & 0 & 0 & 0 \\ 0 & 0 & 0 & 1/G_{yz} & 0 & 0 \\ 0 & 0 & 0 & 0 & 1/G_{zx} & 0 \\ 0 & 0 & 0 & 0 & 0 & 1/G_{xy} \end{bmatrix} \tag{A.1}$$

where the relation $\nu_{ij}/E_i = \nu_{ji}/E_j$ holds (no summation convention implied). An orthotropic material is then fully characterized by nine elastic constants (and three coefficients of thermal expansion). In the case of an organic substrate, we have calculated the quantities relative to the (x, y) plane (i.e. the in-plane properties). For the out-of-plane properties, simple averaging arguments suggest the following definitions:

$$\begin{aligned} E_z &= \left(\sum_{f=1}^{F} \frac{h_f}{h} \frac{1}{E_{z,f}} \right)^{-1} \\ \nu_{xz} &= \sum_{f=1}^{F} \frac{h_f}{h} \nu_{xz,f} \qquad \nu_{yz} = \sum_{f=1}^{F} \frac{h_f}{h} \nu_{yz,f} \\ G_{xz} &= \left(\sum_{f=1}^{F} \frac{h_f}{h} \frac{1}{G_{xz,f}} \right)^{-1} \qquad G_{yz} = \left(\sum_{f=1}^{F} \frac{h_f}{h} \frac{1}{G_{yz,f}} \right)^{-1} \\ \alpha_z &= \sum_{f=1}^{F} \frac{h_f}{h} \alpha_{z,f} \end{aligned} \tag{A.2}$$

where the index f indicates the general layer, F is the total number of layers, h_f is the thickness of layer f and h is the overall thickness of the substrate (or the effective layer being considered).

For each kind of layer (*lines, web* and *vias)*, the effective out-of-plane properties can be modeled as:

(i) *'lines' layers*

$$\begin{aligned} E_3 &= f_{Cu}E_{Cu} + f_{res}E_{res} \approx f_{Cu}E_{Cu} \\ G_{13} &= f_{Cu}G_{Cu} + f_{res}G_{res} \approx f_{Cu}G_{Cu} \\ G_{23} &= \frac{G_{Cu}G_{res}}{f_{Cu}G_{Cu} + f_{res}G_{res}} \\ v_{32} &= v_{12} = f_{Cu}v_{Cu} + f_{res}v_{res} \\ v_{31} &= v_{13} = \frac{f_{Cu}E_{Cu}v_{Cu} + f_{res}E_{res}v_{res}}{f_{Cu}E_{Cu} + f_{res}E_{res}} \\ \alpha_3 &= \frac{f_{Cu}E_{Cu}\alpha_{Cu} + f_{res}E_{res}\alpha_{res}}{f_{Cu}E_{Cu} + f_{res}E_{res}} \end{aligned} \tag{A.3}$$

(ii) *'vias' layers*

$$\begin{aligned} E_3 &\approx f_{Cu}E_{Cu} \\ G_{13} &= G_{23} \approx f_{Cu}G_{Cu} \\ v_{32} &= v_{31} \approx v_{Cu} \\ \alpha_3 &\approx \alpha_{Cu} \end{aligned} \tag{A.4}$$

(iii) *'web' layers*

$$\begin{aligned} E_3 &= f_{Cu}E_{Cu} + f_{res}E_{res} \\ G_{13} &= G_{23} \approx f_{Cu}G_{Cu} \\ v_{31} &= v_{32} \approx v_{Cu} \\ \alpha_3 &= \frac{f_{Cu}E_{Cu}\alpha_{Cu} + f_{res}E_{res}\alpha_{res}}{f_{Cu}E_{Cu} + f_{res}E_{res}} \end{aligned} \tag{A.5}$$

References

[1] Blackshear EB et al. The evolution of build-up package technology and its design challenges. IBM J Res Dev 2005;49:641–61.

[2] Shukla R, Murali V, Bhansali A. Flip chip CPU package technology at Intel: a technology and manufacturing overview. In: Proceedings of the electronic components and technology conference, IEEE; 1999. p. 945–9.

[3] Deasi C, Whitenack R. Review of models and the disturbed state concept for thermomechanical analysis in electronic packaging. ASME J Electron Packag 2001;123:19–33.

[4] Xu B, Cai X, Huang W, Cheng Z. Research of underfill delamination in flip chip by the *J*-integral method. ASME J Electron Packag 2004;126:94–9.

[5] Guven I, Kradinoz V, Tor JL, Madenci E. Strain energy density criterion for reliability and life prediction of solder joints in electronic packaging. ASME J Electron Packag 2004;126:398–405.

[6] Tien JK, Hendrx BC, Attarwala AI. Understanding the cyclic mechanical behavior of lead/tin solder. ASME J Electron Packag 1991;113:115–9.

[7] Paydar N, Tong Y, Akay HU. A finite element study of factors affecting fatigue life of solder joints. ASME J Electron Packag 1994;116:265–73.

[8] Kang SK, Lauro PA, Shih D-Y, Henderson DW, Puttlitz KJ. Microstructure and mechanical properties of lead-free solders and solder joints used in microelectronic applications. IBM J Res Dev 2005;49:607–20.

[9] Desai CS, Wang ZC, Whitenack R, Kundu T. Testing and modeling of solders using new test device, part 1: models and testing. ASME J Electron Packag 2004;126:225–31.

[10] Chiang K-N, Liu C-M. A comparison of thermal stress/strain behavior of elliptical/round solder pads. ASME J Electron Packag 2001;123:127–31.

[11] Sharma P, Dasgupta A. Micro-mechanics of creep-fatigue damage in Pb-Sn solder due to thermal cycling – Part 1: formulation. ASME J Electron Packag 2002;124:292–303.

[12] Suhir E. Modeling of thermal stress in microelectronic and photonic structures: role, attributes, challenges and brief review. ASME J Electron Packag 2003;125:261–7.

[13] Wu L. The thermoelastic analysis of chip-substrate system. ASME J Electron Packag 2004;126:325–32.

[14] Suhir E. Predicted thermal stresses in a bimaterial assembly adhesively bonded at the ends. J Appl Phys 2001;89:120–9.

[15] Suhir E. Interfacial stresses in bimetal thermostats. ASME J Appl Mech 1989;56:595–600.

[16] Tsai MY, Hsu CH, Han CN. A note on Suhir's solution of thermal stresses for a die-substrate assembly. ASME J Electron Packag 2004;126:115–9.

[17] Wen Y, Basaran C. In: Electronics components and technology conference; 2004. p. 1592–601.

[18] Nejhad MNG, Pan C, Feng H. Intrinsic strain modeling and residual stress analysis for thin-film processing of layered structures. ASME J Electron Packag 2003;125:4–17.

[19] Polsky Y, Ume IC. Thermoelastic modeling of a PWB with simulated circuit traces subjected to infrared reflow soldering with experimental validation. ASME J Electron Packag 1999;121:263–70.

[20] Grenestedt JL, Hutapea P. Inflluence of electric artwork on thermo-mechanical properties and warpage of printed circuit boards. J Appl Phys 2003;94:686–96.

[21] Hutapea P, Grenestedt JL, Modi M, Mello M, Frutschy K. Prediction of microelectronic substrate warpage using homogeneized finite element models. Microelectron Eng 2006;83:557–69.

[22] Ubachs RLJM, van der Sluis O, van Driel WD, Zhang GQ. Multiscale modeling of multilayer substrates. Microelectron Reliab 2006;46:1472–7.

[23] Powell PC. Engineering with fibre-polymer laminates. London: Chapman & Hall; 1994.

[24] Torquato S. Random heterogeneous materials. New York: Springer; 2002.

[25] Slaughter WS. The linearized theory of elasticity. Boston: Birkhauser; 2002.